Domain switch toughening in polycrystalline ferroelectrics

Jianxin Wang and Chad M. Landis[a)]
Department of Mechanical Engineering and Materials Science, Rice University, Houston, Texas 77005

(Received 12 July 2005; accepted 1 September 2005)

Mode I steady crack growth was analyzed to determine the toughening due to domain switching in ferroelectric ceramics. A multi-axial, electromechanically coupled, incremental constitutive theory is applied to model the material behavior of the ferroelectric ceramic. The constitutive law is then implemented within the finite element method to study steady crack growth. The effects of mechanical and electrical poling on the fracture toughness are investigated. Results for the predicted fracture toughness, remanent strain distributions, and domain switching zone shapes and sizes are presented. Finally, the model predictions are discussed in comparison discrete switching models and to experimental observations.

I. INTRODUCTION

This paper was presented at the Spring meeting of the Materials Research Society on March 29, 2005 in San Francisco, CA. To place new results in the appropriate context, previously published results are reviewed and cited accordingly.

Ferroelectric ceramics have large electromechanical coupling effects and hence are widely used in smart structure applications. Since these devices often operate under strong mechanical and electrical loading conditions, the brittle ferroelectric material can be susceptible to fracture. Therefore, an understanding of ferroelectric fracture is a key issue for the efficient and reliable design of these devices. There have been numerous experimental investigations on the fracture toughness of ferroelectric ceramics,[1–8] and it is commonly accepted that domain switching leads to increased toughening and R-curve behavior in these materials. It is also well known that both electric field and mechanical stress drive the domain switching process, and hence fracture in ferroelectrics is inherently a coupled electromechanical process. This paper presents a collection of simulation results on the toughening behavior of ferroelectrics undergoing steady crack growth. The unifying feature of these results is the phenomenological constitutive law that is used to represent the electromechanical material response. This constitutive model is incorporated within a steady-state finite element method to determine the domain switch toughening for unpoled, mechanically poled, and electrically poled materials.

II. PHENOMENOLOGICAL CONSTITUTIVE MODEL

The goal of any phenomenological constitutive theory is to provide a relatively simple framework within which the laws of thermodynamics are satisfied and a wide range of material behaviors can be represented. A summary of the recent developments on micro-electromechanical and phenomenological constitutive modeling of ferroelectrics can be found in review articles by Kamlah[9] and Landis.[10] The phenomenological constitutive model presented below is based on the work of Landis and co-workers,[11–13] and additional details of the model can be found in those references. This constitutive model has been verified against experimental observations and micro-electromechanical self-consistent simulations based on the model of Huber et al.[14]

For simplicity, it will be assumed that linear elastic compliances at constant electric field and dielectric permittivity at constant stress are isotropic and not affected by changes in the remanent state of the material. Furthermore, all strain and electric displacement components are referenced from a thermally depolarized state. Under such assumptions, the constitutive relationships are expressed as

$$\epsilon_{ij} = \frac{1+\nu}{\mathrm{E}}\,\sigma_{ij} - \frac{\nu}{E}\,\sigma_{kk}\delta_{ij} + d_{kij}E_k + \epsilon^r_{ij} \quad , \qquad (1)$$

$$D_i = d_{ikl}\sigma_{kl} + \kappa E_i + P^r_i \quad , \qquad (2)$$

where

$$d_{kij} = \frac{d_{33}}{4}\,\frac{P^r}{P_0}\,(3n_i\delta_{jk} + 3n_j\delta_{ik} - 2n_k\delta_{ij}) \quad , \qquad (3)$$

and

$$P^r = \sqrt{P^r_i P^r_i} \qquad \text{and} \qquad n_i = P^r_i/P^r \quad . \qquad (4)$$

a)Address all correspondence to this author.
e-mail: landis@rice.edu
This paper was selected as the Outstanding Meeting Paper for the 2005 MRS Spring Meeting Symposium CC Proceedings, Vol. 881E.
DOI: 10.1557/JMR.2006.0002

Here, ϵ_{ij}, ϵ^r_{ij}, D_i, P^r_i, σ_{ij} and E_i are the Cartesian components of the total strain, remanent strain, electric displacement, remanent polarization, stress, and electric field. The linear material properties are the Poisson's ratio ν, the Young's modulus E, and the dielectric permittivity κ, and δ_{ij} is the Kronecker delta. Finally, d_{33} is the piezoelectric coefficient when P^r reaches the maximum attainable remanent polarization P_0. Note that this form for the piezoelectric coefficients has $d_{31} = -d_{33}/2$ and $d_{15} = 3d_{33}/2$. This is a reasonable assumption based on measured values in polycrystals, and this assumption can be relaxed at the added expense of complexity within the theory.

The purpose of the nonlinear constitutive law is to provide the evolution of the stress, electric field, remanent strain, and remanent polarization histories given the total strain and electric displacement histories. It is assumed that domain switching occurs when a specific switching condition is met. This switching criterion can be used to define a surface in stress and electric field space and will be referred to as the switching surface. The specific form of the switching surface implemented here is that proposed in[11,13]

$$\Phi = \frac{3\hat{s}_{ij}\hat{s}_{ij}}{2\sigma_0^2} + \frac{\hat{E}_i\hat{E}_i}{E_0^2} + \frac{\beta\hat{E}_iP^r_j\hat{s}_{ij}}{E_0P_0\sigma_0} - 1 = 0 \quad , \tag{5}$$

where

$$\hat{\sigma}_{ij} = \sigma_{ij} - \sigma^B_{ij}, \text{ with } \hat{s}_{ij} = \hat{\sigma}_{ij} - \frac{1}{3}\sigma_{kk}\delta_{ij} \text{ and } \hat{E}_i = E_i - E^B_i + \frac{\partial d_{jkl}}{\partial P^r_i}E_j\sigma_{kl} \quad , \tag{6}$$

and σ^B_{ij} is the back stress tensor, E^B_i is the back electric field, σ_0 is the initial switching strength of the material in uniaxial tension or compression, E_0 is the coercive field, and β is a positive scalar parameter. The postulate of maximum dissipation is satisfied if the switching surface is convex and the increments of remanent strain and polarization are normal to the surface. The switching surface defined in Eq. (5) is convex if $\beta < 3$. Normality requires the remanent increments to be given as

$$\epsilon^r_{ij} = \lambda\frac{\partial\Phi}{\partial\hat{\sigma}_{ij}}, \text{ and } P^r_i = \lambda\frac{\partial\Phi}{\partial\hat{E}_i} \quad , \tag{7}$$

where λ is the switching multiplier. To determine the back stress and back electric field, it is assumed that the remanent strain and remanent polarization can be used as internal variables that fully characterize the thermodynamic state of the material. This assumption leads to the identification of a remanent potential, $\Psi^r(\epsilon^r_{ij}, P^r_i)$, such that the back stress and back electric field components can be derived from the potential in the following manner,

$$\sigma^B_{ij} = \frac{\partial\Psi^r}{\partial\epsilon^r_{ij}}, \quad \text{and} \quad E^B_i = \frac{\partial\Psi^r}{\partial P^r_i} \quad . \tag{8}$$

Finally, the form of Ψ^r must be specified to complete the constitutive theory. For the results to be presented, Ψ^r is split into a mechanical part Ψ^σ that enforces the strain saturation conditions, and an electrical part Ψ^E that enforces the polarization saturation conditions, i.e.,

$$\Psi^r = \Psi^\sigma + \Psi^E \quad , \tag{9}$$

$$\Psi^\sigma = \frac{1}{2}H^\sigma_0\epsilon_c\left[\frac{J^e_2}{\epsilon_c}\exp\left(\frac{m}{1-\bar{\epsilon}/\epsilon_c}\right)\right]^2 \quad , \tag{10}$$

where H^σ_0 is a characteristic level of back stress that primarily affects the initial slope of uniaxial stress versus remanent strain curve, and m is another hardening parameter that controls how abruptly the strain saturation conditions can be approached. The multi-axial remanent strain saturation conditions are enforced by causing Ψ^σ to approach infinity as the strain-like variable $\bar{\epsilon}$ approaches the saturation level of remanent strain in uniaxial compression ϵ_c. The effective saturation remanent strain quantity $\bar{\epsilon}$ is defined as

$$\bar{\epsilon} = J^e_2 f(J^e_3/J^e_2) \quad , \tag{11}$$

where

$$f\left(\frac{J^e_3}{J^e_2}\right) = -0.0965\left(\frac{J^e_3}{J^e_2}\right)^3 + 0.01\left(\frac{J^e_3}{J^e_2}\right)^6 + 0.8935, \text{ for } \left(\frac{J^e_3}{J^e_2}\right) < 0 \quad , \tag{12}$$

and

$$f\left(\frac{J^e_3}{J^e_2}\right) = -0.1075\left(\frac{J^e_3}{J^e_2}\right)^3 - 0.027\left(\frac{J^e_3}{J^e_2}\right)^6 - 0.028\left(\frac{J^e_3}{J^e_2}\right)^{21} + 0.8935, \text{ for } \left(\frac{J^e_3}{J^e_2}\right) \geqslant 0 \quad . \tag{13}$$

Here, f is a functional fit to the numerical results obtained from the micromechanical computations described in Ref. 12. The following remanent strain invariants appearing in Eqs. (11)–(13) are used to describe the multi-axial remanent strain state

$$J^e_2 = \left(\frac{2}{3}e^r_{ij}e^r_{ij}\right)^{1/2} \text{ and } J^e_3 = \left(\frac{4}{3}e^r_{ij}e^r_{jk}e^r_{ki}\right)^{1/3} \quad , \tag{14}$$

where e^r_{ij} is the remanent strain deviator, $e^r_{ij} = \epsilon^r_{ij} - \delta_{ij}\epsilon^r_{kk}/3$.

Next, the electrical part of Ψ^r has the form of

$$\Psi^E = H^E_0P_0\left[\ln\left(\frac{1}{1-P^r/P_{sat}}\right) - \frac{P^r}{P_{sat}}\right] \quad , \tag{15}$$

where

$$P_{sat} = \frac{3P_0}{4(\epsilon_t + \epsilon_c)}(\epsilon^r_{ij}n_in_j + \epsilon_c) + \frac{P_0}{4} \quad . \tag{16}$$

Here ϵ_t is the remanent saturation strain in uniaxial tension and according to Eqs. (10)–(13) is equal to 1.368 ϵ_c. The maximum attainable remanent polarization P_0 has been defined previously. Note that the level where the remanent polarization saturates P_{sat} is a function of the remanent strain and the maximum of P_0 can only be attained if $\epsilon^r_{ij} n_i n_j = \epsilon_t$. If $\epsilon^r_{ij} n_i n_j = -\epsilon_c$ then the maximum level for P^r is only $P_0/4$. This result and the linear approximation to the functional form for P_{sat} given in Eq. (16) are taken directly from the micro-electromechanical computations described in Ref. 13. A more detailed description of the model can be found in Refs. 11–13, and examples of the constitutive response are illustrated in Figs. 1(a)–1(d). The material properties used for these simulations are characteristic of a soft lead lanthanum zirconate titanate (PLZT) material as measured by Lynch[15] and are specifically given as: $\sigma_0 =$ 27.5 MPa, $E_0 = 0.35$ MV/m, $P_0 = 0.26$ C/m^2, $\epsilon_c =$ 0.0012, $\beta = 2.95$, $\kappa = 6 \times 10^{-8}$ C/(m·V), $E = 70$ GPa, $\nu = 0.4$, $d_{33} = 3 \times 10^{-10}$ m/V, $d_{31} = -(d_{33}/2)$, $m =$ 0.01, $H^\sigma_0 = 0.5\sigma_0$, $H^E_0 = 0.05\ E_0$.For the numerical implementation of the constitutive model into the finite element model, a backward Euler integration routine was developed to solve the constitutive equations. The scheme is similar to that described in Refs. 16–18.

III. FRACTURE MODEL

In this work Mode I steady crack growth is analyzed in mechanically poled and electrically poled ferroelectric materials. For each of the situations to be modeled, a schematic of the geometry and loading is illustrated. Initially, the samples are poled by applying a uniaxial electric field (electrical poling) or a uniaxial stress (mechanical poling) and then removing the applied load. The electrical poling process induces both an initial residual remanent polarization $P^{r,0}_i$ and initial remanent strain $\epsilon^{r,0}_{ij}$ in the material as referenced from the thermally depolarized state. The mechanical poling process induces only an initial remanent strain $\epsilon^{r,0}_{ij}$. In simulations with an

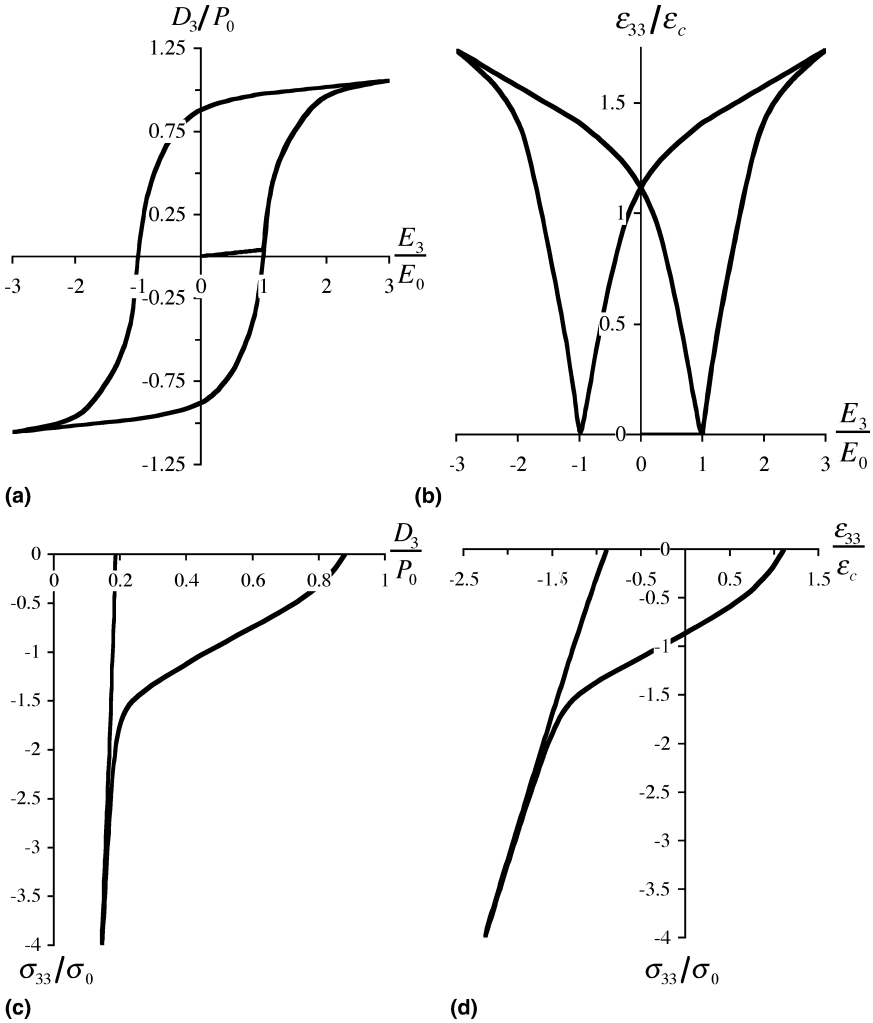

FIG. 1. (a) Uniaxial electric displacement D_3 versus electric field E_3 hysteresis loop. (b) Uniaxial strain ϵ_{33} versus E_3 butterfly loop. (c) Depolarization due to compressive stress σ_{33}. (d) Stress versus strain during depolarization.

additional applied electric field, uniform electric field boundary conditions are applied to the outer boundary after the initial poling process. The final step in the loading process is to apply the in-plane mechanical loads. Under plane-strain conditions the out-of-plane axial strain ϵ_{33} is assumed to remain unchanged from its state after the secondary electrical loading step, i.e., $\epsilon_{33} = \epsilon_{33}^0$. Steady crack growth then occurs while the in-plane mechanical loads are applied.

During crack growth, small scale switching will be assumed such that the representative height of the nonlinear switching zone near the crack tip is much smaller than any other characteristic specimen dimension such as crack length, specimen width, or ligament width. Furthermore, under plane-strain conditions, it is assumed that the specimen thickness is much greater than the switching zone size as well. The assumption of small scale switching will not be valid for cases when switching occurs over the entire sample. However, it is assumed here that for such cases the in-plane applied mechanical loads can still be characterized by a Mode I K-field (appropriately modified for the effects of piezoelectricity[19]), and this K-field determines the mechanical loading applied to the outer boundary. Finally, the applied steady state energy release rate G_{ss} is equal to $(1 - \nu^2)K^2/E$ for materials with in-plane isotropy, and the exact relationship between G_{ss} and K can be found in Ref. 19 when there is in-plane piezoelectricity. Note that G_{ss} is determined by the specified applied loading and is not changed by the nonlinear features of the solution.

The remaining analysis will focus on the toughening due to domain switching during the steady crack growth. Under steady growth conditions, all increments of field quantities can be related to derivatives with respect to the x_1 coordinate direction, i.e., the crack growth direction, by

$$\chi = -\dot{a}\,\frac{\partial \chi}{\partial x_1} \quad . \tag{17}$$

Here, χ is any scalar field quantity such as a Cartesian component of remanent strain or remanent polarization, and is the increment of crack advance in the $\dot{a}$ direction. Within the fracture model, crack propagation is assumed to occur when the crack tip energy release rate G_{tip} reaches a critical value. To compute the relationship between the applied steady state energy release rate G_{ss} and G_{tip}, a steady state finite element formulation is implemented to determine the electromechanical fields.[16–18] Then, under steady-state conditions, G_{tip} can be calculated using the electromechanical form of Hutchinson's I-integral:[20]

$$G_{tip} = I \equiv \int_S (Hn_1 - \sigma_{ij} n_j u_{i,1} + D_i n_i E_1)\mathrm{d}S \quad , \tag{18}$$

where S is a surface enclosing the crack tip, n_i are the components of the unit normal directed outward from the surface, u_i are the components of the displacement vector, D_i are the components of the electric displacement vector, E_1 is the electric field in x_1 direction, and H is the history dependent electric enthalpy density at a material point defined by

$$H = \int_0^{\epsilon_{ij}, E_i} \sigma_{ij}\mathrm{d}\epsilon_{ij} - D_i \mathrm{d}E_i \quad . \tag{19}$$

The calculation of G_{tip} is carried out after the finite element solution is obtained.

To compute the electromechanical fields numerically, the following finite element formulation is applied. If we assume that the free charge density in the volume is equal to zero, the vector potential formulation described in Ref. 21 can be used. The finite element formulation required to solve the steady crack growth boundary value problem is based on the variational statement

$$\int_V \sigma_{ij}\delta\epsilon_{ij} + E_i \delta D_i \mathrm{d}V = \int_s T_i \delta u_i + \phi\delta\omega \mathrm{d}S \quad . \tag{20}$$

Full details of the finite element procedure can be found elsewhere.[16–18,21] Equation (20) is solved with an iterative technique. To begin, uniform remanent strain and polarization distributions are assumed. Next, the system of finite element equations is solved to obtain a new but approximate solution for the nodal unknowns. A new approximate strain and electric displacement distribution is derived from these nodal unknowns. Then the incremental constitutive model described previously is integrated along streamlines of constant height above the crack plane from $x = +\infty$ to $x = -\infty$ to obtain updated approximations for the stress, electric field, remanent strain, remanent polarization, and piezoelectric property distributions. The new remanent strain and remanent polarization distributions are then applied within the next finite element solution, and the solution/streamline integration procedure is repeated until a suitable level of convergence is achieved. Once convergence is obtained, the crack tip energy release rate is computed from Eq. (18) using the domain integral technique.[22]

IV. RESULTS

Results are presented to illustrate the influence of mechanical and electrical poling on the fracture behavior of ferroelectric materials. As mentioned previously, the primary result from each steady crack growth calculation is the ratio of the far field applied energy release rate G_{ss} to the crack tip energy release rate G_{tip}. However, prior to presenting results for the relative level of toughening for different poling states, some features of the switching zones near the crack tip will be given first.[16]

Figure 2 plots contours of normalized remanent strain around a steadily growing crack in an initially unpoled material loaded only by mechanical stresses.

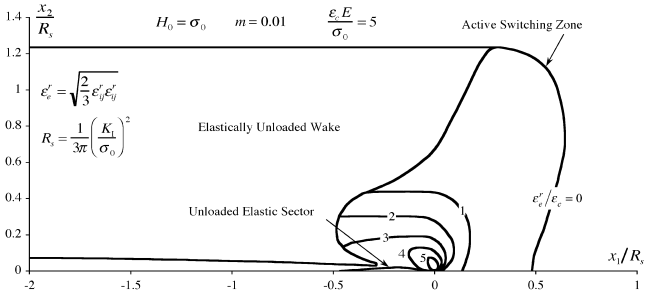

FIG. 2. Domain switching zone around a steadily growing crack in an initially unpoled material subjected to an applied *K*-field. Only the upper half-plane is depicted.

In Fig. 2, the outer solid line delineates the boundary between material that is undergoing changes in remanency due to domain switching and material that is not. It is worth noting that the sizes of the inner contours where the effective remanent strain is most intense are significantly smaller than the outer switching zone boundary. This feature is to be expected but cannot be captured by simpler "discrete switching" constitutive models where the material cannot exist in an intermediate remanent state. This illustrates the fact that intense domain switching is confined to a region very close to the crack tip. Furthermore, note that the shape of the switching zone depicted here is that of the active switching zone. In other words, in the active switching zone, neighboring points at the same height above the crack plane have different remanent strain and polarization states. In the linearly unloaded wake, however, neighboring points at the same height above the crack plane have identical remanent states. To restate, the primary difference between these results and previous toughening calculations based on discrete switching models is that the incremental constitutive model is able to account for and predict the inhomogeneous remanent state within the switching zone around the crack tip.

Recall that within the fracture model it is assumed that crack growth occurs when G_{tip} reaches the intrinsic fracture toughness of the material G_0. Hence the ratio G_{ss}/G_0 indicates the amount of toughening due to domain switching, with $G_{\text{ss}}/G_0 = 1$ corresponding to no toughness enhancement or R-curve behavior. With regard to R-curve behavior, G_0 should be interpreted as the applied energy release rate where crack growth first begins, and G_{ss} is the steady state or plateau level of the applied energy release rate after a sufficient amount of crack growth.

The first set of switch toughening results to be presented in Fig. 3 are for the case of "mechanical poling."[17] In this situation, the material is first loaded by a uniaxial stress in either tension or compression and then unloaded producing an initial remanent strain state in the material. After the initial poling load is removed, the *K* field is applied and crack growth proceeds under plane strain conditions.

Based on the intuitive ideas that the crack tends to cause switching towards the *y*-direction and a greater potential for switching towards the *y*-direction should yield a tougher material, the results for the X and Y-poled material are to be expected. However, one might expect that the Z-poled material should produce a similar behavior as the X-poled material based on these considerations since both situations have exactly the same propensity for switching towards the *y*-direction. However, the reason why the toughening of the Z-poled material exhibits less sensitivity to the initial remanent strain state is due to the plane strain constraint. Specifically, the approaching crack does create a driving force for switching from the *z* orientation to the *y* orientation. However, if this switch does occur, then large axial stresses will be generated in the *z* direction due to the plane strain constraint, and these stresses will tend to oppose the switch towards the *y* orientation. The net effect is that only a moderate amount of switching occurs for the Z-poled material, and the full potential of the domain switch toughening is not realized.

The next set of results to be presented are for materials with remanent poling due to electric field and applied electric field in the out-of-plane direction.[18] The material properties used for these simulations are characteristic of a soft PLZT material as measured by Lynch[15] and were specifically given prior to the presentation of Fig. 1.

Figure 4 on the next page illustrates the geometry and loading for the out-of-plane electrical loading cases and the associated results for the toughening as a function of applied electric field. Note that the features of the toughening butterfly loop correspond to the features of the strain butterfly loop. In general, when the electric field is in the same direction as the polarization, the domain switch toughening is reduced, and when the electric field opposes the remanent polarization, the toughening is enhanced. Again, this feature is to be expected by realizing that an electric field parallel to the remanent polarization will retard switching to the in-plane directions while an anti-parallel field will enhance such switching. With respect to fracture toughness, more switching and dissipation implies more toughening. As for the mechanically poled case, the counterintuitive result that the poled material (outer butterfly loop curves) has approximately the same toughening as the unpoled material (inner curve) under no applied electric field appears. Again, this feature can be explained by considering the effects of the plane strain constraint. Quantitative results on the effects of plane strain versus plane stress are presented in the next set of figures.

The final set of results is for initial remanent polarization and strain with no applied electric field after the initial poling process. For the simulations with

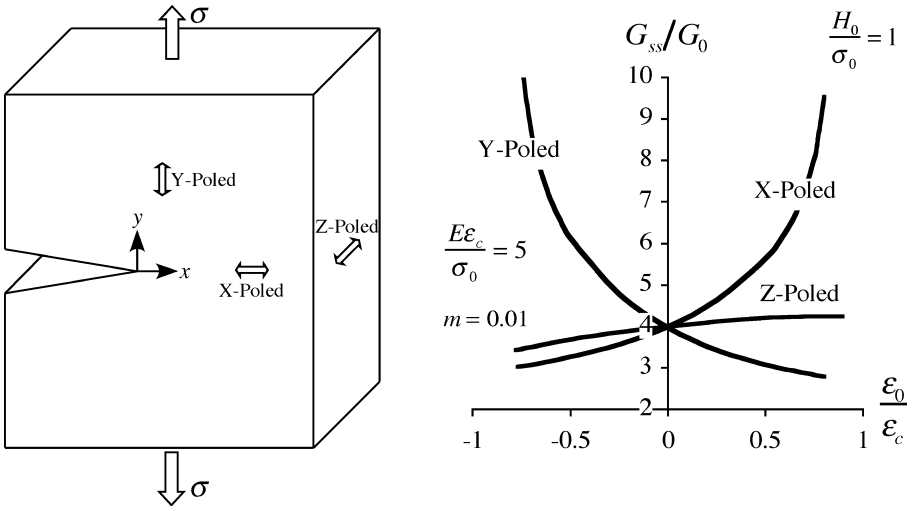

FIG. 3. Domain switch toughening ratio in plane strain as a function of initial uniaxial remanent strain for the three different poling directions.

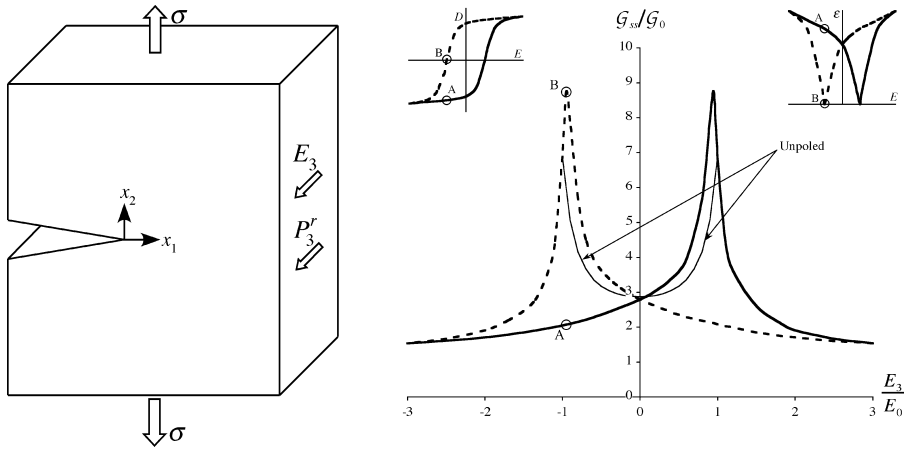

FIG. 4. Domain switch toughening butterfly loop for a material with initial remanent polarization and applied electric field parallel to the crack front.

polarization in the plane of mechanical loading, permeable electrical boundary conditions have been applied on the crack faces. Such electrical crack face boundary conditions are valid if the electric breakdown field within the crack gap is assumed to be small.[23] Figure 5(a) illustrates that as the initial remanent polarization state increases, the toughening will increase for poling parallel to the crack surface, decrease for poling perpendicular to the crack surface, and is relatively flat for poling parallel to the crack front. Some experimental observations have indicated that the greatest toughening occurs for poling in the x_3 direction.[6] However, this behavior is observed only if the electrodes on the x_3 surfaces are removed prior to the application of the mechanical loads. When, the electrodes remain on the specimen and are short-circuited, as modeled here, the toughening for x_3-poled specimens is similar to that of unpoled samples[6,8] as predicted by this model. The explanation for this behavior is again due to the effects of the plane strain constraint. To validate this hypothesis, Fig. 5(b) illustrates the effects of plane stress versus plane strain on the toughening. It is clear from Fig. 5(b) that the unintuitive results seen in Figs. 3–5—(i.e., that the out-of-plane poled materials are not significantly tougher than the unpoled materials)—are in fact due to the out-of-plane constraint imposed by the plane strain conditions.

V. DISCUSSION

The model presented here differs from previous theoretical explanations of the effects of electric field and remanent state on the fracture toughness of ferroelectrics in that an incremental, micro-electromechanically informed, phenomenological constitutive law has been applied instead of a discrete switching law. Additionally, in contrast to applying simplifying assumptions about the distributions of the fields, which are associated with most transformation toughening models, the details of the electromechanical fields have been explicitly obtained from finite element computations. The fields computed

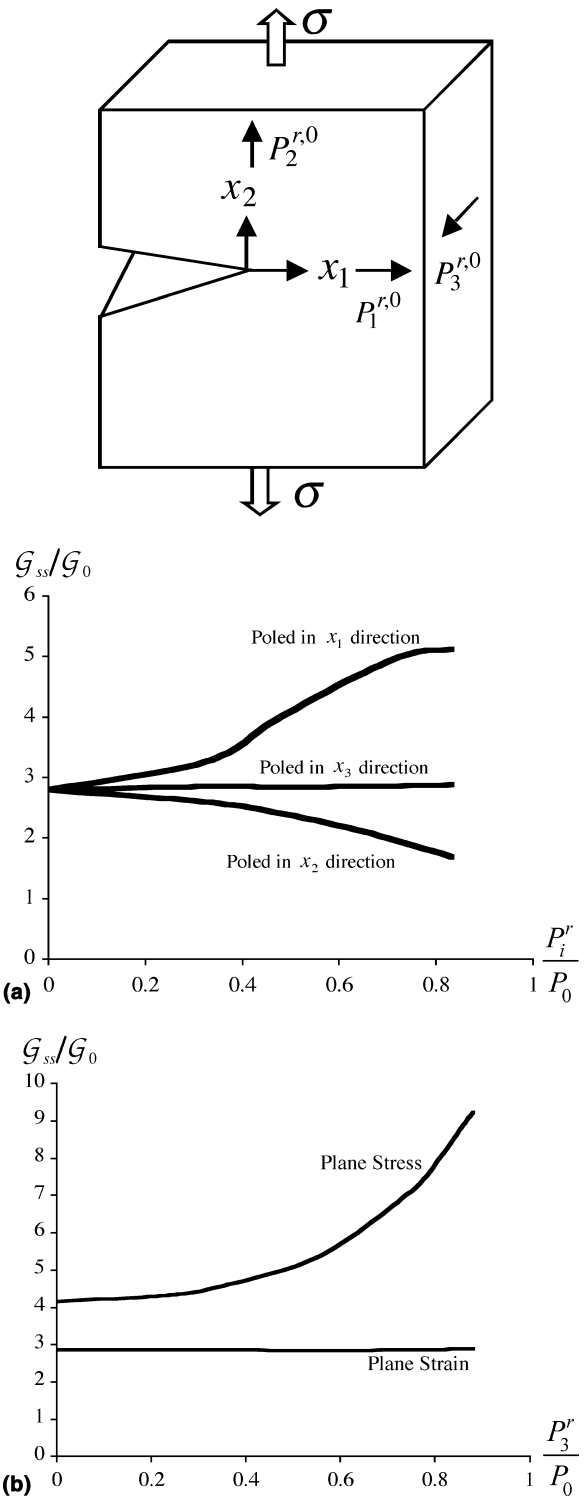

FIG. 5. Domain switching toughening as a function of initial remanent polarization magnitude for (a) plane strain and three different poling directions and (b) plane stress versus plane strain for the out-of-plane poling direction.

in this work include both the perturbing influences of ferroelectric switching and the changes in the piezoelectric effect that results from such switching. The constitutive model applied in this work has allowed for both qualitative and quantitative characterizations of the effects of electrical and mechanical poling on the toughening due to domain switching in ferroelectric ceramics. The model predicts a range of phenomena that indicate that the toughening is dependent on both the level of initial remanent poling state and on the poling direction. As a complement to qualitative characterizations, the quantitative predictions of the model allow for a direct comparison to some recent experimental studies.

For the in-plane poling case, the present model predicts what experiments[1–7] have indicated, that poling parallel to the crack surface yields higher toughening than poling perpendicular to the crack surface. Ultimately, the present model predicts a range of effects of poling in different directions on the fracture toughness, or more specifically, the toughening due to domain switching during crack growth. The model predicts the unintuitive behavior that the fracture toughness of a material poled out-of-plane is comparable to the toughness of an initially unpoled material. It was demonstrated that this behavior is primarily due to the out-of-plane mechanical constraint imposed by plane strain conditions. This prediction has previously been confirmed experimentally[6,8] and cannot be predicted by discrete switching models.

ACKNOWLEDGMENT

The authors would like to acknowledge support from the Army Research Office.

REFERENCES

1. G.G. Pisarenko, V.M. Chusko, and S.P. Kovalev: Anisotropy of fracture toughness of piezoelectric ceramics. *J. Am. Ceram. Soc.* **68,** 259 (1985).
2. K. Metha and A.V. Virkar: Fracture mechanisms in ferroelectric-ferroelastic lead zirconate titanate (Zr:Ti = 0.54:0.46) ceramics. *J. Am. Ceram. Soc.* **73,** 567 (1990).
3. A.G. Tobin and Y.E. Pak: Effect of electric fields on fracture behavior of PZT ceramics. *Proc. SPIE* **1916,** 78 (1993).
4. H. Wang and R.N. Singh: Crack propagation in piezoelectric ceramics: Effects of applied electric field. *J. Appl. Phys.* **81,** 7471 (1997).
5. G.A. Schneider and V. Heyer: Influence of the electric field on Vickers indentation crack growth in $BaTiO_3$. *J. Eur. Ceram. Soc.* **19,** 1299 (1999).
6. S.L. Lucato, J. Lindner, D.C. Lupascu, and J. Rödel: Influence of electrical and geometrical boundary conditions on crack growth in PZT. *Key Eng. Mater.* **206–213,** 609 (2002).
7. W. Yang, F. Fang, and M. Tao: Critical role of domain switching on the fracture toughness of poled ferroelectrics. *Int. J. Solids Struct.* **38,** 2203 (2001).
8. S. Hackemann and W. Pfeiffer: Domain switching in process zones of PZT: Characterization by micro diffraction and fracture mechanical methods. *J. Eur. Ceram. Soc.* **23,** 141 (2003).
9. M. Kamlah: Ferroelectric and ferroelastic piezoceramics—modeling and electromechanical hysteresis phenomena. *Continuum Mech. Thermodyn.* **13,** 219 (2001).

10. C.M. Landis: Non-linear constitutive modeling of ferroelectrics. *Curr. Opin. Solid State Mater. Sci.* **8,** 59 (2004).
11. C.M. Landis: Fully coupled, multi-axial, symmetric constitutive laws for polycrystalline ferroelectric ceramics. *J. Mech. Phys. Solids* **50,** 127 (2002).
12. C.M. Landis: On the strain saturation conditions for polycrystalline ferroelastic materials. *J. Appl. Mech.* **70,** 470 (2003).
13. C.M. Landis, J. Wang, and J. Sheng: Micro-electromechanical determination of the possible remanent strain and polarization states in polycrystalline ferroelectrics and implications for phenomenological constitutive theories. *J. Intell. Mater. Syst. Struct.* **15,** 513 (2004).
14. J.E. Huber, N.A. Fleck, C.M. Landis, and R.M. McMeeking: A constitutive model for ferroelectric polycrystals. *J. Mech. Phys. Solids* **47,** 1663 (1999).
15. C.S. Lynch: The effect of uniaxial stress on the electro-mechanical response of 8/65/35 PLZT. *Acta Mater.* **44,** 4137 (1996).
16. C.M. Landis: On the fracture toughness of ferroelastic materials. *J. Mech. Phys. Solids* **51,** 1347 (2003).
17. C.M. Landis: On the fracture toughness anisotropy of mechanically poled ferroelectric ceramics. *Int. J. Fract.* **126,** 1 (2004).
18. J. Wang and C.M. Landis: On the fracture toughness of ferroelectric ceramics with electric field applied parallel to the crack front. *Acta Mater.* **52,** 3435 (2004).
19. C.M. Landis: In-plane complex potentials for a special class of materials with degenerate piezoelectric properties. *Int. J. Solids Struct.* **41,** 695 (2004).
20. J.W. Hutchinson: "A course on nonlinear fracture mechanics," *Harvard University Report, DEAP S-8*, Division of Applied Sciences (Harvard University, Cambridge, MA, 1974).
21. C.M. Landis: A new finite-element formulation for electromechanical boundary value problems. *Int. J. Numer. Meth. Eng.* **55,** 613 (2002).
22. F.Z. Li, C.F. Shih, and A. Needleman: Comparison of methods for calculating energy release rates. *Eng. Fract. Mech.* **21,** 405 (1985).
23. C.M. Landis: Energetically consistent boundary conditions for electromechanical fracture. *Int. J. Solids Struct.* **41,** 6291 (2004).